Effect of Growth Temperature on Composition Control for Vapor Deposition of $YBa_2Cu_3O_{7-\delta}$ Precursor Films

Chong Liu, Lianhong Wang, Yonghua Shu and Jing Fan

State Key Laboratory of High-temperature Gas Dynamics, Institute of Mechanics, Chinese Academy of Sciences, Beijing 100190, China

Abstract. This work aims at exploiting the role of growth temperature on the dynamic behavior of deposition atoms as well as its resultant impact on the composition control during the synthesis of $YBa_2Cu_3O_{7-\delta}$ precursor films by vapor codeposition. The codeposition of Yt, BaF_2 and Cu is performed in vacuum chamber under a wide range of growth temperature from 25℃ to 600℃, the mass of each element deposited on $LaAlO_3$ substrate and thus the film composition is examined by the inductively coupled plasma atomic emission spectroscopy. It is shown that the deposition amount of Cu decreases obviously with the increase of growth temperature; however, the mass of Yt and BaF_2 deposited on the substrate appears to be insensitive to growth temperature. Moreover, high temperature may also trigger the influence of adsorbates composition on Cu desorption, and therefore the deposition amount of Cu decreases almost linearly as the mol fraction of BaF_2 in the adlayers increases. Nevertheless, when the deposition is conducted at room temperature, the influence of mol fraction of BaF_2 on Cu desorption vanishes. The detailed mechanisms associated with above phenomena are unveiled by molecular dynamics analysis, additionally the physical picture about adsorption behaviors on the growing interface under different deposition conditions is summarized, which is valuable for handling the composition control during the vapor codeposition of different functional films.

Keywords: Composition control, growth temperature, $YBa_2Cu_3O_{7-\delta}$ precursor films, vapor deposition.
PACS: 34.35.+a, 68.43.-h, 74.72.-h

INTRODUCTION

Nanofilms with novel physical properties play crucial role in many functional devices [1]. Much effort has therefore been attracted on the synthesis of new functional nanofilms in both scientific research and industrial applications [1, 2]. Unlike the widely used structure material, nanofilms are usually employed as functional material, and accordingly the research focus for nanofilms is shifted from the mechanical properties to the intriguing physical properties as well as its applications[3-7]. Most of the functional nanofilms are multi-component compounds, different species of atoms and ions are bonded and connected with each other, and then the atomic structure is formed [8, 9]. Actually, the novel functional properties of nanofilms arise from its individual atomistic geometry and bonding characteristics, which can be greatly altered by the change of material compositions [10-12]. Therefore, the composition of nanofilms is vital to its functional applications, and hence it is important to precisely control its composition during the film synthesis.

The vapor codeposition techniques are good at mixing the deposited elements, and thus it has become one of the most versatile approaches to synthesize functional nanofilms [1, 13]. Our previous experiment shows that the film composition can be well controlled on condition that the vapor codepositions are performed under room temperature, i.e., without external substrate heating. However, to synthesize some particular functional crystals, the deposited atoms have to undergo reconstruction to build the desired nanostructure through sufficient atomic diffusion [8], which requires that the substrate should be heated and kept at certain temperature during codepositions [14]. In addition, high temperature can also help the deposited atoms to overcome large potential barrier for different reactions, and consequently facilities the formation of the expected functional crystal. With above physical considerations, high temperature deposition is indispensible for the synthesis of some nanofilms. As a matter of fact, when the substrate is maintained at high temperature, the competition of kinetic energy of adatoms with the surface binding energy makes the dynamics of adsorbates adjacent to the growing interface more complicated [15-17], which may cause a lot of desorptions and make troubles to the composition control [18, 19]. To circumvent this problem, the influence of growth temperature on the dynamic behaviors of atoms to be and has been deposited under different conditions need to be well studied.

Proceedings of the 29th International Symposium on Rarefied Gas Dynamics
AIP Conf. Proc. 1628, 439-445 (2014); doi: 10.1063/1.4902626
© 2014 AIP Publishing LLC 978-0-7354-1265-1/$30.00

In this work, a series of experiments for the vapor codeposition of Yt, BaF_2 and Cu are performed under a wide range of temperature. The results indicate that the deposition amount of Cu decreases obviously with the increase of the growth temperature; however, for BaF_2 and Cu, the deposition amount does not change too much within the experimental temperature range from 25℃ to 600℃. Moreover, another interesting thing is also observed, i.e., the deposition amount of Cu decreases almost linearly with the increases of the atomic fraction of BaF_2, when the deposition temperature is low, the deposition amount of Cu becomes insensitive to the atomic fraction of BaF_2 in the adlayers. The mechanisms behind these phenomena are disclosed by the molecular dynamic analysis. The physical picture about the detailed dynamic processes on the growing interface under different deposition conditions is unveiled, which provides valuable information for the film composition control in vapor codeposition under high temperatures.

EXPERIMENT

The vapor codeposition system utilized in this work consists of a vacuum chamber, monitors and controlling devices. To guarantee high performance of the electron gun and large mean free path for the delivery the evaporated atoms, the background pressure in vaccuum chamber is usually maintained below 3×10^{-3} Pa during deposition. The vacuum chamber is divided into different regions, in each region the evaporation source is placed inside the crucible, as shown by the schematic in Fig. 1. The evaporation of Yt and Cu is heated by electron guns and the thermal resistance heater is used to evaporate BaF_2. The quartz crystal oscillator fixed in each region is employed as a sensor to detect the impinging flux of the individual source, it sends back signal to the thin film deposition controller. By comparing the detected flux with the desired value, the controller will send command to increase or reduce the power of the electron-gun, and therefore the evaporation rate. Through this approach, the incident flux evaporated from different sources can be well controlled at a fixed value.

The precursor films of YBCO are deposited on 15×5 mm^2 (100) $LaAlO_3$ substrates, which are fixed on a substrate disk in the top region of the vacuum chamber, as illustrated by the green slice in Fig. 1. Prior to loading on the substrate disk, the $LaAlO_3$ substrate is cleaned with acetone, ethanol, diluted phosphoric acid, deionized water, and subsequently dried with N_2 gas. The temperature of the substrate is monitored by pyrometer. During codeposition, as the disk rotates around its axis, the substrates pass through different evaporation regions and expose to the impinging flux of different sources alternatively. Therefore, the elements from different evaporation sources can be uniformly mixed on the substrates. After each deposition, the mass of each element deposited on the substrate can be obtained by the inductively coupled plasma atomic emission spectroscopy (ICP-AES) analysis.

The codeposition of Yt, BaF_2 and Cu are performed with different substrate temperatures form 25 ℃ to 600 ℃. For the purpose of exploring the pure effect of growth temperature, we keep other deposition conditions unchanged from run-to-run, e.g., the impinging flux in each evaporation region. Only for some occasional case, the deposition time (deposition thickness on the controller) is reduced by a half or the substrate size is two times larger (15×10).

The precursor films of YBCO are deposited on 15×5 mm^2 (100) $LaAlO_3$ substrates, which are fixed on a substrate disk in the top region of the vacuum chamber, as illustrated by the green slice in Fig. 1. Prior to loading on the substrate disk, the $LaAlO_3$ substrate is cleaned with acetone, ethanol, diluted phosphoric acid, deionized water, and subsequently dried with N_2 gas. The temperature of the substrate is monitored by pyrometer. During codeposition, as the disk rotates around its axis, the substrates pass through different evaporation regions and expose to the impinging flux of different sources alternatively. Therefore, the elements from different evaporation sources can be uniformly mixed on the substrates. After each deposition, the mass of each element deposited on the substrate can be obtained by the inductively coupled plasma atomic emission spectroscopy (ICP-AES) analysis.

The codeposition of Yt, BaF_2 and Cu are performed with different substrate temperatures form 25 ℃ to 600 ℃. For the purpose of exploring the pure effect of growth temperature, we keep other deposition conditions unchanged from run-to-run, e.g., the impinging flux in each evaporation region. Only for some occasional case, the deposition time (deposition thickness on the controller) is reduced by a half or the substrate size is two times larger (15×10 mm^2), the effect of this difference needs to be considered during the experimental data analysis. Since the deposition amount has linear relation with deposition time and substrate area, and hence the mass of each element deposited on substrate could be scaled by the area of substrate and deposition thickness on thin film deposition controller. The reduced deposition mass of each element (φ) is plotted as a function of substrate temperature in Fig. 2, it is seen that as temperature increases, the deposition amount of Cu decreases. Nevertheless, for BaF_2 and Yt, φ does not change too much with temperature. This means that the role of growth temperature on deposition is not sensitive for all of the evaporation sources, which is intriguing enough to merit detailed investigations.

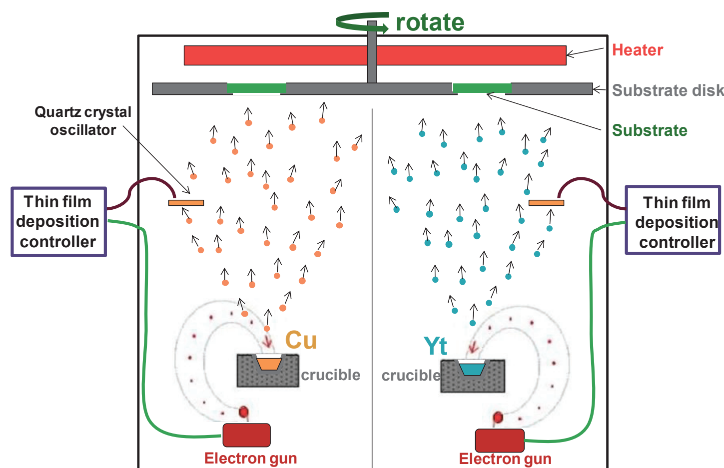

FIGURE 1. The schematic illustration of the key instruments in the film deposition systems. It is noted that in real experiment system, the vacuum chamber is divided into three evaporation regions for Yt , Cu and BaF_2 respectively. Here only two of them (for Cu and Yt) are illustrated.

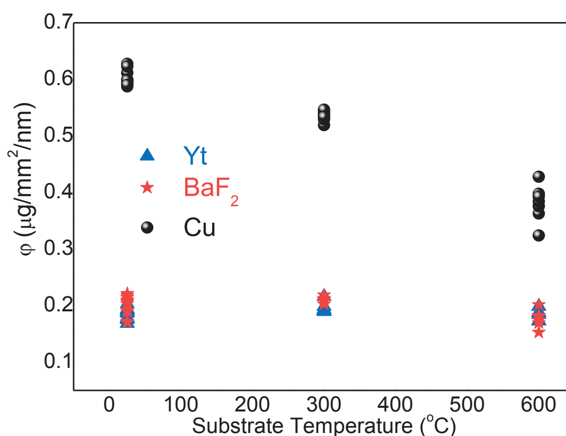

FIGURE 2. The deposition amount of the Yt, BaF_2 and Cu on $LaAlO_3$ substrate versus substrate temperature. To exclude the effect of substrate size and deposition time, the deposition amount is scaled by the substrate area and deposition thickness of each element on the quartz crystal thin films deposition controller.

MOLECULAR DYNAMICS SIMULATION

To understand above phenomena, molecular dynamics (MD) simulation is performed to study the physical process on the growing interface during depositions by using the Large scale Atomic/Molecular Massively Parallel Simulator (LAMMPS) [20, 21].The MD simulation system consists of a substrate and the atoms to be or has been deposited [22], as shown in Fig. 3. The embedded-atom method (EAM) force field is employed to consider the thermal vibration of the substrate atoms [23], which affect the energy accommodation of substrate atoms and the dynamics of the deposited atoms on the substrate. The deposited atoms is modeled by the Lennard-Jones (LJ) potential, $U(r) = 4\varepsilon[(\sigma/r)^{12} - (\sigma/r)^{6}]$, where r is the separation between a pair of molecules, σ is the collision diameter, and ε is the binding energy. The interaction between the deposition atoms and the substrate atoms is also calculated by LJ potential, and the Lorentz-Berthelot mixing rule is used to calculate the interaction parameters. In order to implement the mixing rule for the interaction, we use the LJ parameters given in Ref. [24] for the adsorbates (deposition atoms) and substrate. To explore the surface effects on substrate, the adsorbate-substrate binding energy is arbitrarily varied in MD simulation.

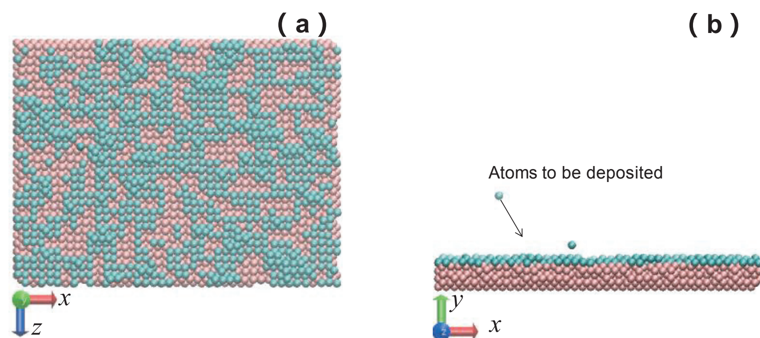

FIGURE 3. Structure of the molecular dynamics simulation model. The red particles are the substrate atoms and the green one represents the atoms have been or to be deposited. (a) Top view and (b) Front view.

The planar substrate perpendicular to the *y* axis is placed at the bottom of the simulation box [Fig.3(b)]. Six layer of body center cubic (bcc) Fe atoms are used to model the substrate surface, the typical system is shown in Fig.3 (b). The atoms in the bottom-most layer is fixed to maintain a stable system, and the atoms in the other layer are free to vibrate to simulate to thermal motion of surface atoms. The size of the substrate is about 11.4nm×8.6nm which along *x* and *z* directions respectively, and the length of the simulation system in the *y* direction is about 8.6 nm. Periodic boundary conditions are applied in the *x* and *z* directions only, to simulate to desorption and reevaporation processes, an imagine boundary is assumed on top boundary of the system (parallel to the substrate surface and perpendicular to *y* axis).When the atoms inside the simulation system go across this imagine boundary, the simulation will stop tracking the position of these atoms beyond the imagine boundary. The atoms to be deposited are inserted randomly in the top region of the simulation box; an initial velocity in negative *y* direction is assigned to each inserted deposition atoms. Besides the deposition atoms, random initial velocities that follow the Maxwell – Boltzmann distribution corresponding to the desired temperature are assigned to the substrate atoms. The Nose – Hoover thermostat is employed to control temperature of substrate at the desired values.

The deposition process under different temperatures and surface binding are explored by MD simulations. The adsorption probability is estimated by the number of deposited atoms actually adsorbed on the substrate divided by the number of total atoms has ever collided with the growing interface. Figure 4 illustrates that as the growing temperature increases the adsorption probability is reducing from 1 to 0, which indicates a transition from the complete adsorption region to no adsorption region. It is also noted that when the surface binding is weak, this transition takes place at low temperature region; however, for the strong surface binding, this transition shifted towards high temperature, which may beyond the range of deposition temperature, as shown by the red curve in Fig.4.

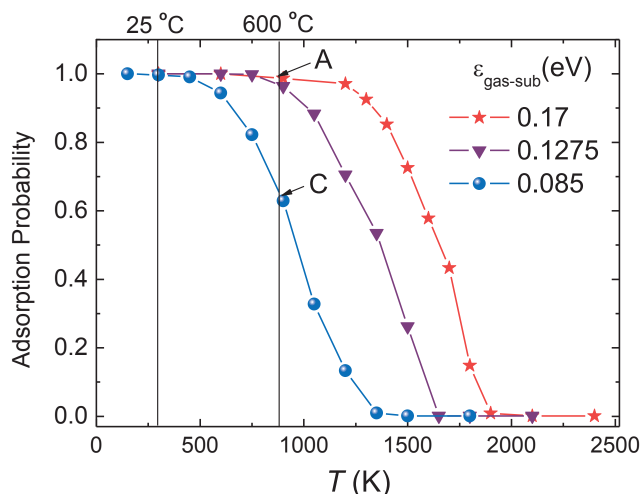

FIGURE 4. Adsorption probability of Cu as a function of growth temperature under various gas-substrate binding strength. The results are obtained from molecular dynamics simulations.

Compared with Copper (Cu), Yttrium and Barium are much easier to be oxidized [25, 26], which indicates that barium and yttrium are more prone to connect with negative ions (e.g., the oxygen ions O^{-2} or the fluoride ions F^{-1}) by chemical bond. With this consideration, the chemical adsorption is favorable for Yt and Ba. Typically, the binding strength of chemical adsorption is much stronger than that of physical adsorption where the Van der Waals' force is dominant [18]. For strong binding case, as shown by the red curve in Fig. 4, the transition from complete adsorption to no adsorption takes place at high temperature region, within the deposition temperature range (from 25℃ to 600℃) the adsorption probability does not change too much. That's why the deposition amount of Yt and BaF_2 is insensitive to temperature. On the other hand, since the surface binding for Cu is much weaker, the transition from adsorption region to no adsorption occurs under low temperature, which is within deposition temperature range, and consequently the adsorption probability can be obviously reduced by increasing temperature, as shown by the blue curve in Fig. 4. As a result, the deposition amount of Cu decreases with increasing temperature. This in turn verifies our previous, yet preliminary, interpretation that the trouble in the composition control for high-temperature deposition is caused by desorption behavior depends which can be greatly affected by both the growth temperature and surface binding strength.

EXTENDED ANALYSIS AND DISCUSSIONS

Besides the effect of temperature, another interesting phenomenon is also observed. As illustrated in Fig. 5(a), the deposition amount of Cu decreases almost linearly with the increase of the Mol fraction of BaF_2, which indicates that the deposition amount of Cu can be greatly altered by the composition of the previously deposited adsorbates. This is completely unexpected by us, and requires extended detailed analysis on the surface binding. In initial deposition stage, the substrate surface is almost clear, and the dominant surface binding is the gas-substrate binding which is determined by the interaction between gas atoms to be deposited and substrate surface atoms. As the deposition goes on, the substrate will be covered by a thicker layer of mixed atoms or molecules, which separate the direct interaction between gas atoms and substrate [27]. Therefore, in the full coverage stage, the dominant surface binding becomes gas-adsorbate binding which depends on the interactions between the atoms to be deposited and the atoms have already been deposited on the growing interface [28]. In this case, the strength of the gas-adsorbate binding is not only dependent on the type of atoms to be deposited [29], but also influenced by the composition change in the adsorbates [30].

Since the composition variations may alter the atomistic structure and bonding characteristic, and consequently the surface binding energy. From the results in Fig. 5(a), we can speculate that the decrease of atomic fraction of BaF_2 may weaken the binding between the gas atoms and adsorbates. As a result, the transition from complete adsorption to no adsorption in Fig. 4 will be shifted by the change of surface binding, e.g., from the red curve to the blue curve. When the deposition temperature is fixed, for instance 600℃ in Fig. 4, the weakened surface binding could reduce the adsorption probability from point A to point C, as shown in Fig.4. As a consequence, the deposition amount of Cu decreases with the increase of mol fraction of BaF_2.

When the experiment is conducted under room temperature, the deposition amount of Cu becomes insensitive to growth temperature, as shown in Fig. 5(b). Under low temperature, all the curve of adsorption probability for different binding energies converge to unity, no matter how large the surface binding energy can be altered by the adsorb rates composition, the adsorption probability does not change (see Fig.4). That's why for room temperature deposition, the deposition amount of Cu becomes insensitive to the mol fraction of BaF_2.

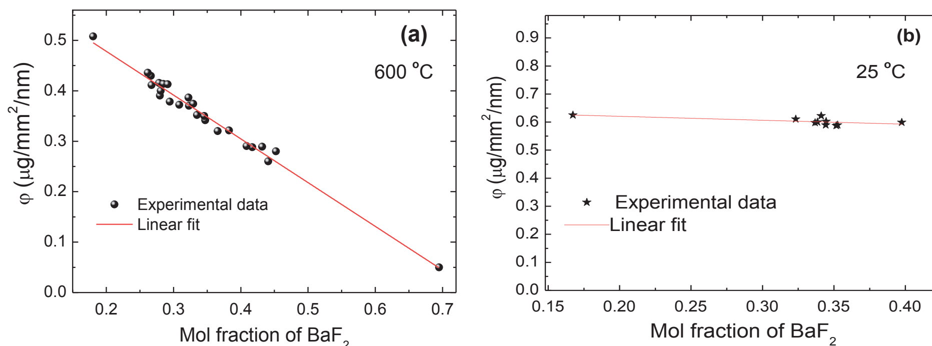

FIGURE 5. The deposition amount of Cu versus the mol fraction of BaF_2. The deposition amount is scaled by the substrate area and deposition thickness on the quartz crystal thin films deposition controller. （a）600℃ and (b) 25 ℃.

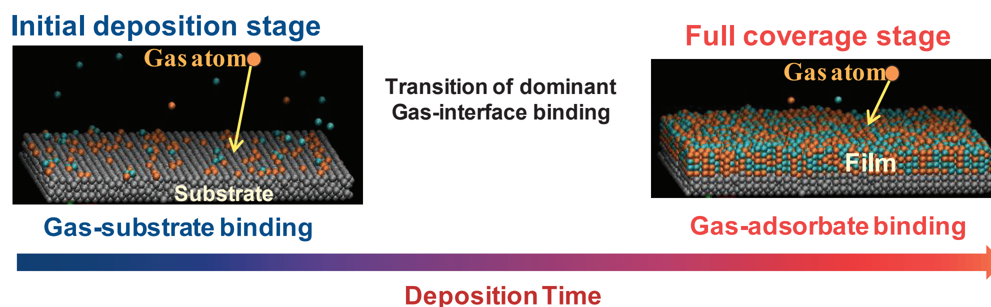

FIGURE 6 The schematic show of the transition from initial deposition stage to the full coverage stage.

CONCLUSION

In summary, the vapor codeposition of Yt, BaF_2 and Cu are carried out under a wide range of growth temperature from 25℃ to 600℃. The experimental results combined with MD analysis indicate that only for the elements bears weak surface binding, such as Cu, the deposition amount is sensitive to the growth temperature due to the desorption triggered by the increase of substrate temperature. However, for Yt and BaF_2 the strong chemical binding suppress high temperature induced desorption, and therefore the deposition amount becomes temperature independent. More interestingly, we observed that the deposition amount may also be influenced by the change of the atomic fraction of BaF_2 in the adlayer on condition that surface binding of the deposition element is weak and the growth temperature is high. As the atomic fraction of BaF_2 in the precursor films increases, the deposition amount of Cu atoms decreases obviously, this could be attributed to the change of surface binding. At low temperature, the influence of BaF_2 atomic fraction on the desorption probability of Cu vanishes. The above information is valuable for the film composition control in vapor codepositions under high temperature.

ACKNOWLEDGMENTS

This work is supported by the National Natural Science Foundation of China (Grants No. 11302227).

REFERENCES

1. S. Zhang, Nanostructured Thin Films and Coatings: Functional Properties, New York: CRC Press, 2010.
2. C. Cepek, R. Macovez, M. Sancrotti, L. Petaccia, R. Larciprete, S. Lizzit, and A. Goldoni, *Appl. Phys. Lett.* **85** 976-978 (2004).
3. D. V. Talapin and C. B. Murray, *Science* **310** 86-89 (2005).
4. H. Byrd, E. P. Suponeva, A. B. Bocarsly, and M. E. Thompson, *Nature* **380** 610-612 (1996).
5. F. B. Abdelrazzaq, R. C. Kwong, and M. E. Thompson, *J. Am. Chem. Soc.* **124** 4796-4803 (2002).
6. X. L. Zhong, J. B. Wang, M. Liao, L. Z. Sun, H. B. Shu, C. B. Tan, and Y. C. Zhou, *Appl. Phys. Lett.* **90** 102906 (2007).
7. A. Gozar, G. Logvenov, L. F. Kourkoutis, A. T. Bollinger, L. A. Giannuzzi, D. A. Muller, and I. Bozovic, *Nature* **455** 782-785 (2008).
8. C. Liu, J. Zhang, l. Wang, Y. Shu, and J. Fan, *Solid State Ionics* **232** 123-128 (2013).
9. L. Wang, Y. Shu, and J. Fan, *Sci. China-Technol. Sci.* **55** 2291-2294 (2012).
10. R. Jaafar, D. Berling, D. Sebilleau, and G. Garreau, *Phys. Rev. B* **81** (2010).
11. C. S. Lue, Y. S. Tseng, J. Y. Huang, H. L. Hsieh, H. Y. Liao, and Y. K. Kuo, *AIP Adv.* **3** (2013).
12. A. Kawano, H. Ishiwata, S. Iriyama, R. Okada, T. Yamaguchi, Y. Takano, and H. Kawarada, *Phys. Rev. B* **82** (2010).
13. J. Fan, I. D. Boyd, and C. Shelton, *J. Vac. Sci. Technol. A* **18** 2937-2945 (2000).
14. Y. Han, B. Uenal, and J. W. Evans, *Phys. Rev. Lett.* **108** (2012).
15. J. Zhu, P. Goetsch, N. Ruzycki, and C. T. Campbell, *J. Am. Chem. Soc.* **129** 6432-6441 (2007).
16. T. Karabacak, H. Guclu, and M. Yuksel, *Phys. Rev. B* **79** (2009).
17. H. J. Kim, Y. Egashira, and H. Komiyama, *Appl. Phys. Lett.* **59** 2521-2523 (1991).

18. N. Lopez, F. Illas, and G. Pacchioni, *J. Am. Chem. Soc.* **121** 813-821 (1999).
19. Y. D. Kim, T. Wei, S. Wendt, and D. W. Goodman, *Langmuir* **19** 7929-7932 (2003).
20. B. C. Hubartt, X. Liu, and J. G. Amar, *J. Appl. Phys.* **114** (2013).
21. http://lammps.sandia.gov/index.html.
22. J. Zhang, C. Liu, Y. Shu, and J. Fan, *Appl. Surf. Sci.* **261** 690-696 (2012).
23. M. S. Daw and M. I. Baskes, *Phys. Rev. Lett.* **50** 1285-1288 (1983).
24. P. M. Agrawal, B. M. Rice, and D. L. Thompson, *Surf. Sci.* **515** 21-35 (2002).
25. J. Li, J. W. Mayer, and E. G. Colgan, *J. Appl. Phys* **70** 2820-2827 (1991).
26. M. Gurvitch, L. Manchanda, and J. M. Gibson, *Appl. Phys. Lett.* **51** 919-921 (1987).
27. A. Beniya, K. Mukai, Y. Yamashita, and J. Yoshinobu, *J. Chem. Phys.* **129** (2008).
28. R. Friedlein, A. Fleurence, J. T. Sadowski, and Y. Yamada-Takamura, *Appl. Phys. Lett.* **102** (2013).
29. Y. Kitaguchi, S. Habuka, T. Mitsui, H. Okuyama, S. Hatta, and T. Aruga, *J. Chem. Phys.* **139** (2013).
30. L. W. Liu, K. Yang, W. D. Xiao, Y. H. Jiang, B. Q. Song, S. X. Du, and H. J. Gao, *Appl. Phys. Lett.* **103** (2013).

AIP Conference Proceedings is copyrighted by AIP Publishing LLC (AIP). Reuse of AIP content is subject to the terms at: http://scitation.aip.org/termsconditions. For more information, see http://publishing.aip.org/authors/rights-and-permissions.